

Path radiance technique for retrieving aerosol optical thickness over land

Guoyong Wen,¹ Si-Chee Tsay,² Robert F. Cahalan,^{1,2} and Lazaros Oreopoulos¹

Abstract. The key issue in retrieving aerosol optical thickness over land from shortwave satellite radiances is to identify and separate the signal due to scattering by a largely transparent aerosol layer from the noise due to reflection by the background surface, where the signal is relatively uniform compared to the highly inhomogeneous surface contribution. Sensitivity studies in aerosol optical thickness retrievals reveal that the apparent reflectance at the top of the atmosphere is very susceptible to the surface reflectance, especially when aerosol optical thickness is small. Uncertainties associated with surface reflectance estimation can greatly amplify the error of the aerosol optical thickness retrieval. To reduce these uncertainties, we have developed a “path radiance” method to retrieve aerosol optical thickness over land by extending the traditional technique that uses the “dark object” approach to extract the aerosol signal. This method uses the signature of the correlation of visible and middle-IR reflectance at the surface and couples the correlation with the atmospheric effect. We have applied this method to a Landsat TM (Thematic Mapper) image acquired over the Oklahoma southern Great Plains site of the Department of Energy Atmospheric Radiation Measurement (ARM) program on September 27, 1997, a very clear day (aerosol optical thickness of 0.07 at 0.5 μm) during the first Landsat Intensive Observation Period. The retrieved mean aerosol optical thickness for TM band 1 at 0.49 μm and band 3 at 0.66 μm agree very well with the ground-based Sun photometer measurements at the ARM site. The ability to retrieve small aerosol optical thickness makes this path radiance technique promising. More importantly, the path radiance is relatively insensitive to surface inhomogeneity. The retrieved mean path radiances in reflectance units have very small standard deviations for both TM blue and red bands. This small variability of path radiance further supports the current aerosol retrieval method.

1. Introduction

Atmospheric aerosols are a source of major uncertainty in better understanding our climate system, due mainly to the large spatial and temporal variability of their microphysical properties and chemical composition. Aerosols are liquid and solid particles suspended in the air from natural or man-made sources [Kaufman *et al.*, 1997a]. Aerosols may modulate the climate system directly by scattering and absorbing solar and terrestrial radiation and, indirectly, by serving as cloud condensation nuclei to influence cloud microphysics and hence cloud radiative properties [Intergovernmental Panel on Climate Change (IPCC), 1996, and references therein]. To assess the climatic impact of aerosol on a global scale, a variety of instruments designed for measuring different aerosol properties are now and/or will soon be flying on spacecraft (cf. Kaufman *et al.* [1997a, 1998] for a more detailed review).

Aerosol retrieval over oceans has been studied extensively by utilizing the low reflectance of oceans at solar wavelengths, especially in the red and near-infrared regions [e.g., Fraser, 1976; Mekler *et al.*, 1977; Köpke and Quenzel, 1979, 1981; Käst-

ner *et al.*, 1983; Griggs, 1983; Stowe *et al.*, 1997; Tanré *et al.*, 1997; Nakajima and Higurashi, 1997]. Only recently has special attention been focused on aerosol retrieval over land where most anthropogenic aerosol arises [e.g., Kaufman and Sendra, 1988; Fraser *et al.*, 1992; Liang *et al.*, 1997; Kaufman *et al.*, 1997b].

Both the atmosphere and the surface reflectance affect the solar radiation remotely sensed by satellite. Aerosols are optically thin in most geographic locations except in strong source regions. Large spatial and temporal variability in surface reflectance makes the optical thickness retrieval of this largely transparent medium very difficult over land. Thus aerosol retrieval and atmospheric correction for surface characterization are intimately coupled.

Earlier research on aerosol retrieval over land for a polluted, hazy atmosphere used clear atmosphere in the same region as the reference [Fraser *et al.*, 1984; Kaufman *et al.*, 1990; Ferrare *et al.*, 1990]. The technique assumes the surface reflectance to be the same as that on a clear day with low aerosol loading. In order to reduce surface effects, Kaufman and Sendra [1988] suggested a “dark object” approach to retrieve aerosol optical thickness in regions where the surface is covered with dense vegetation or forest. One advantage of the dark object approach is that the surface reflectance is small, so that the error in retrieved aerosol optical thickness is also relatively small compared to errors over bright surfaces. Another advantage of using the dark object approach is that there are correlations between the middle-IR band at 2.2 μm and visible (blue and

¹Joint Center for Earth Systems Technology, University of Maryland Baltimore County, Catonsville.

²NASA Goddard Space Flight Center, Greenbelt, Maryland.

Copyright 1999 by the American Geophysical Union.

Paper number 1999JD900964.
0148-0227/99/1999JD900964\$09.00

red) bands. Hence the middle-IR band may be used to estimate the surface reflectance in the blue and red bands and, further, to infer aerosol optical thickness in the two bands [Kaufman *et al.*, 1997b]. However, application of the technique is not straightforward because the relationship between the middle-IR and visible bands (e.g., blue and red) changes with time and varies from one type of vegetation to another, and within certain types of vegetation, as the internal structure of chlorophyll and water amount changes. A departure from the “mean relation” leads to a bias.

To effectively use the estimated surface reflectance to retrieve aerosol optical thickness, we need to answer three questions: How sensitive is apparent reflectance to the uncertainty of the surface reflectance estimate? How does the variability of surface reflectance and aerosol optical thickness contribute to the apparent reflectance? How can errors in surface reflectance be translated to errors in retrieved aerosol optical thickness? To answer these questions, we first present in section 2 a series of sensitivity studies based on detailed radiative transfer calculations. Section 3 then presents the theoretical basis of the method used to retrieve aerosol optical thickness over land. Section 4 describes the retrieval algorithm in detail and applies it to a Landsat-5 TM scene over the southern Great Plains (SGP) site in Oklahoma, acquired on September 27, 1997, during the Atmospheric Radiation Measurement (ARM) fall Intensive Operation Period (IOP). Section 5 compares retrieved aerosol optical thickness with ground-based Sun photometer measurements and with those retrieved from the “dark object” approach. Errors in aerosol optical thickness are also estimated. A brief summary and discussion of this study is given in section 6.

2. Radiative Transfer Sensitivity Study

Solar radiation reaching the Earth’s atmosphere experiences scattering and absorption by both aerosols and molecules in the atmosphere and reflection at the surface. The remotely sensed radiation in turn may be used to infer the atmospheric constituents and surface properties. Landsat TM band 1 at 0.49 μm (blue band) and band 3 at 0.66 μm (red band) have been used to retrieve aerosol optical thickness by using middle-IR at 2.2 μm to estimate surface reflectance [Kaufman *et al.*, 1997b; Liang *et al.*, 1997]. This section provides a sensitivity study of aerosol optical thickness retrieved in these two TM bands.

2.1. Radiative Transfer and Aerosol Models

Sensitivity is determined from a series of radiative transfer calculations, using a one-dimensional discrete ordinate radiative transfer model [Stamnes *et al.*, 1988; Tsay *et al.*, 1990]. A midlatitude summer standard atmosphere and continental aerosol model [d’Almeida *et al.*, 1991; Shettle and Fenn, 1979; Tsay *et al.*, 1991] with plane parallel stratification are employed. The aerosol particulate is assumed to be spherical. Mie theory is used to calculate single-scattering albedo and scattering phase function. The surface is assumed to be a Lambertian reflector. The atmosphere is assumed to be clear, and this paper deals with cloudless conditions exclusively. Spectral response functions of the various thematic mapper (TM) bands [Markham and Barker, 1985] are used to simulate satellite-observed radiances.

Even though the one-dimensional radiative transfer model accurately describes the radiation field in a plane parallel atmosphere, the inhomogeneities of surface reflectance over

land can affect the accuracy of the one-dimensional (1-D) approximation. Earlier studies demonstrated that adjacency effects can blur the high-resolution satellite images [e.g., Oortman and Fraser, 1979; Mekler and Kaufman, 1980; Tanré *et al.*, 1981; Diner and Martonichik, 1985]. In regions with large contrast in surface reflectance such as near coastlines, the radiances from the one-dimensional plane parallel radiative transfer model may be biased. However, for irregular land surfaces, relatively accurate results can be produced even by the one-dimensional radiative transfer model due to the cancellation from darker and brighter surfaces. The spherical harmonic discrete ordinate method (SHDOM) for 3-D atmospheric radiative transfer [Evans, 1998] is used to perform a sensitivity study on the effects of surface inhomogeneity on the backscattered radiation. The 2-D surface reflectance is assumed to be randomly distributed ranging from 0 to 0.2 with 30 m grid size and periodic boundary condition. Molecular scattering is included with the aerosol optical thickness of 0.2 for both TM blue and red bands and solar zenith angle of 45°. Compared with the 3-D SHDOM results, we found the apparent nadir reflectance from 1-D model for both TM bands to deviate by less than 0.015 over darker or brighter surfaces. These differences are reduced to less than 0.01 when the top and bottom 20 percentile of the pixels are excluded.

The radiance $I(\mu_0, \phi_0, \mu, \phi)$ at the top of the atmosphere may be scaled to apparent reflectance as follows:

$$\alpha(\mu_0, \phi_0, \mu, \phi) = \pi I(\mu_0, \phi_0, \mu, \phi) / \mu_0 F_0, \quad (1)$$

where μ_0, μ are cosines of solar zenith and satellite zenith angle, and ϕ_0, ϕ are solar and satellite azimuth angles, and F_0 is the solar extraterrestrial spectral irradiance. The wavelength dependence is left out for simplicity. For Landsat TM measurements close to nadir view, $\mu \approx 1$ and $\phi_0 \approx \phi \approx 0$. A typical solar zenith angle of 45° is used to represent a midlatitude situation.

2.2. Sensitivity due to Variability of Optical Thickness and Surface Reflectance

For the purpose of this sensitivity study, we assume that satellite-observed apparent reflectance is only a function of aerosol optical thickness and surface reflectance with everything else fixed. For an atmosphere with aerosol optical thickness τ_0 and surface reflectance ρ_0 , the apparent reflectance due to uncertainties $\Delta\tau$ and $\Delta\rho$ may be approximated by Taylor expansion

$$\alpha(\tau, \rho) = \alpha(\tau_0, \rho_0) + \frac{\partial\alpha}{\partial\tau} \Delta\tau + \frac{\partial\alpha}{\partial\rho} \Delta\rho, \quad (2)$$

where

$$\tau = \tau_0 + \Delta\tau, \quad \rho = \rho_0 + \Delta\rho \quad (3)$$

when $\Delta\tau$ and $\Delta\rho$ are small. The change of apparent reflectance comes from the change due only to the aerosol optical thickness (the second term on the right-hand side of (2)) and the change due only to the surface reflectance (the third term on the right-hand side of (2)). The two partial derivatives $\partial\alpha/\partial\tau$ and $\partial\alpha/\partial\rho$ describe the sensitivity of apparent reflectance due to aerosol optical thickness and surface reflectance, respectively, and are plotted in Figures 1 and 2.

Both partial derivatives are functions of aerosol optical thickness and surface reflectance. For a given aerosol optical thickness, $\partial\alpha/\partial\tau$ (Figure 1) monotonically decreases with surface reflectance, showing that apparent reflectance is less sen-

sitive to aerosol optical thickness when the surface is brighter. For a given surface reflectance, $\partial\alpha/\partial\tau$ first increases with optical thickness, reaching a maximum at optical thickness about 0.7, and then decreases with optical thickness. The increase of $\partial\alpha/\partial\tau$ for small aerosol optical thickness is associated with the increase of multiple scattering as aerosol optical thickness increases. As aerosol optical thickness further increases, the transmittance decreases exponentially, and apparent reflectance starts to saturate, hence $\partial\alpha/\partial\tau$ also decreases. The value of $\partial\alpha/\partial\tau$ ranges from 0.05 to 0.09 when the surface reflectance ranges from 0 to 0.12, and the aerosol optical thickness ranges from zero to 2.

The partial derivative $\partial\alpha/\partial\rho$ describes the sensitivity of apparent reflectance to surface reflectance (Figure 2). It varies from about 0.3 to 0.9 for both blue and red bands for the ranges of surface reflectance and aerosol optical thickness shown. For a given surface reflectance, $\partial\alpha/\partial\rho$ decreases monotonically with aerosol optical thickness; that is, the dependence of apparent reflectance on surface reflectance weakens as aerosol optical thickness increases. For a given aerosol optical thickness, $\partial\alpha/\partial\rho$ increases slowly with surface reflectance, showing the larger contribution from a brighter surface. The $\partial\alpha/\partial\tau$ is about 0.65 to 0.9 for aerosol optical thickness less than 0.5. With thicker aerosol optical thickness, greater than 1.5, $\partial\alpha/\partial\rho$ is less than 0.4 for both blue and red bands.

For the same aerosol optical thickness and surface reflectance, the apparent reflectance is more sensitive to surface reflectance in the red band than in the blue band. This is

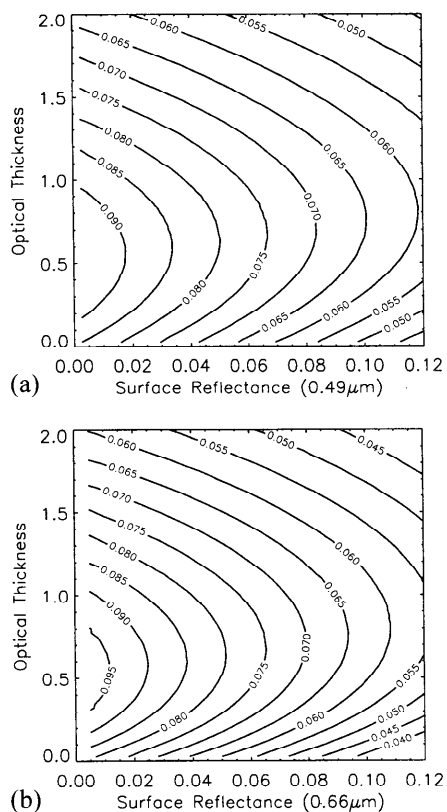


Figure 1. Partial derivative of apparent reflectance with respect to aerosol optical thickness for (top) Landsat TM band 1 at $0.49 \mu\text{m}$ and (bottom) band 3 at $0.66 \mu\text{m}$ from radiative transfer calculation. A summer midlatitude atmosphere, and continental aerosol model, is used with solar zenith angle of 45° .

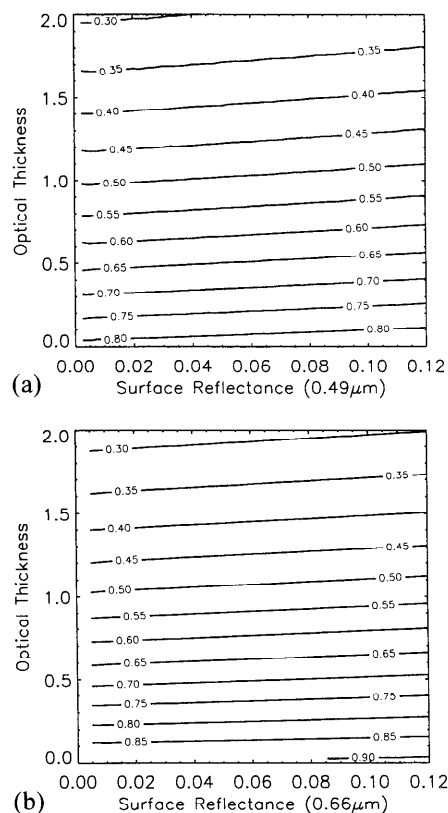


Figure 2. Partial derivative of apparent reflectance with respect to surface reflectance for (top) Landsat TM band 1 at $0.49 \mu\text{m}$ and (bottom) band 3 at $0.66 \mu\text{m}$ from radiative transfer calculation for the atmosphere defined in Figure 1.

because molecular scattering is much less pronounced in the red band.

2.3. Error Budget Analysis

Aerosol optical thickness retrieval typically requires knowledge of surface reflectance. Uncertainties in surface reflectance lead to errors in aerosol optical thickness retrieval. Suppose the real aerosol optical thickness is τ_0 , and the real surface reflectance is ρ_0 . The apparent reflectance $\alpha(\tau, \rho)$ is equated to the observed $\alpha(\tau_0, \rho_0)$ in the retrieval process, so that the error in ρ implies an error in computed τ . The relation between the two uncertainties due to error propagation may be derived from (1):

$$\Delta\tau = -E\Delta\rho \quad (4)$$

where

$$E = \frac{\partial\alpha}{\partial\rho} / \frac{\partial\alpha}{\partial\tau}. \quad (5)$$

The error propagation factor E , which is a function of aerosol optical thickness and surface reflectance, is computed from the radiative transfer model described in section 2.1 and displayed in Figures 3a and 3b for the blue and red bands, respectively.

The positive sign of E in both blue and red indicates the compensating effect of ρ and τ . For example, an underestimate of surface reflectance results in an overestimate in aerosol optical thickness, adjusted to match the apparent reflectance at the top of the atmosphere. Similarly, an overestimate of sur-

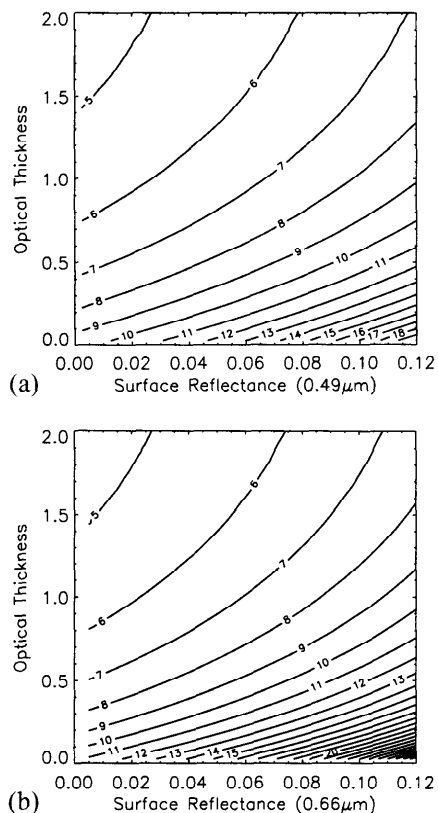


Figure 3. Error propagation factor E defined by equation (5) and computed from radiative transfer calculation for (top) Landsat TM band 1 at $0.49 \mu\text{m}$ and (bottom) band 3 at $0.66 \mu\text{m}$ for the atmosphere defined in Fig. 1.

face reflectance requires an underestimate of aerosol optical thickness to produce the same apparent reflectance as observed.

For both blue and red bands, the error propagation factor decreases monotonically with optical thickness for a given surface reflectance, showing less surface effect as aerosol optical thickness increases. The error propagation factor increases monotonically with surface reflectance for a given aerosol optical thickness because of the larger contribution for a brighter surface. The uncertainty in aerosol optical thickness is about 5–20 times the surface reflectance uncertainty for the range of aerosol optical thickness and surface reflectance considered.

The error propagation factor is larger for the red band than the blue band, especially for small aerosol optical thickness. This is because molecular scattering is much less effective in the red wavelengths than in the blue wavelengths, so the red band is more closely related to the surface reflectance.

The error in surface reflectance is amplified to an error in aerosol optical thickness when aerosol optical thickness is small over a brighter surface. For instance, with surface reflectance of 0.05 at $0.49 \mu\text{m}$ and 0.1 at $0.66 \mu\text{m}$, with aerosol optical thickness of 0.2, an error of 0.015 in surface reflectance will lead to aerosol optical thickness uncertainties of 0.15 in the blue band and 0.25 in the red band. Even for a darker surface, 0.025 at $0.49 \mu\text{m}$ and 0.05 at $0.66 \mu\text{m}$, for example, with a smaller aerosol optical thickness of 0.1, a one-third uncertainty in blue and one-fourth uncertainty in red will result to uncertainties of 0.08 and 0.16, respectively, still significant.

To reduce uncertainties in aerosol optical thickness retrieval and, consequently, reduce uncertainties in atmospheric correc-

tion, we developed a path radiance technique that couples the aerosol effects with the surface reflectance for Landsat TM images. The retrieval scheme uses the fact that correlations exist between the middle-IR band at $2.2 \mu\text{m}$ and the visible (blue $0.49 \mu\text{m}$ and red at $0.66 \mu\text{m}$) bands for land surfaces, particularly over wet soil and vegetated surfaces as in the dark object technique of Kaufman *et al.* [1997b]. However, we do not assume universal relations, thus allowing for the spatial and temporal dependence of the correlations.

3. Theoretical Basis

Satellite-observed solar radiation is the integrated result of all possible effects in the atmosphere-surface coupled system. Sometimes signal from one source dominates others. The signal then can be used to retrieve characteristics of the source with high confidence. The retrieval of aerosol optical thickness over ocean is a good example of the atmospheric contribution dominating over that from the surface. Aerosol optical thickness retrieval over land, by contrast, is more complex. In this situation, signals from aerosols and surface are difficult to separate. However, it is still possible to infer aerosol information if the surface reflectance has certain characteristics.

3.1. Theory

Atmospheric aerosols not in a strong source regions tend to be horizontally stratified. With a horizontally homogenous aerosol layer, we expect the apparent reflectance of visible and middle IR to be linearly correlated if the surface reflectance of the two bands is linearly correlated. To give a simple explanation, we may express the apparent reflectance at visible wavelengths α_{vis} as

$$\alpha_{\text{vis}} = \alpha_{\text{vis}}^{\text{atm}} + T_{\text{vis}}(\mu_0)T_{\text{vis}}(\mu)\rho_{\text{vis}}/(1 - \rho_{\text{vis}}R), \quad (6)$$

where $\alpha_{\text{vis}}^{\text{atm}}$ is the path radiance in reflectance units, $T_{\text{vis}}(\mu_0)$ is the transmittance of solar radiation to the surface for cosine of solar zenith angle μ_0 , $T_{\text{vis}}(\mu)$ is the transmittance of surface upwelling radiation to the top of the atmosphere for satellite-viewing direction μ , ρ_{vis} is the surface reflectance, and R is the diffuse reflectance of the atmosphere [Liou, 1980]. For middle-IR wavelengths, where atmospheric scattering can be ignored for most aerosol types (smoke, sulfates, etc.) [Kaufman *et al.*, 1997b], the apparent reflectance of the middle IR may be expressed as

$$\alpha_{2.2\mu\text{m}} = T_{2.2\mu\text{m}}(\mu_0)T_{2.2\mu\text{m}}(\mu)\rho_{2.2\mu\text{m}}, \quad (7)$$

where the notation is similar to that in (6).

When $\rho_{\text{vis}}R$ is small, which holds for blue and red bands over wet soil and vegetation, (6) may be approximated as

$$\alpha_{\text{vis}} \approx \alpha_{\text{vis}}^{\text{atm}} + T_{\text{vis}}(\mu_0)T_{\text{vis}}(\mu)\rho_{\text{vis}}. \quad (8)$$

Suppose the surface reflectance of the visible and the middle-IR bands are related by

$$\rho_{\text{vis}} = \xi\rho_{2.2\mu\text{m}}, \quad (9)$$

then the apparent reflectance observed from satellite is

$$\alpha_{\text{vis}} \approx \alpha_{\text{vis}}^{\text{atm}} + \frac{T_{\text{vis}}(\mu_0)T_{\text{vis}}(\mu)}{T_{2.2\mu\text{m}}(\mu_0)T_{2.2\mu\text{m}}(\mu)} \xi\alpha_{2.2\mu\text{m}}. \quad (10)$$

Therefore the apparent reflectances of the visible and the middle-IR bands are linearly correlated if their surface counterparts are linearly correlated.

3.2. Radiative Transfer Calculations

The relationship between the visible (blue and red) and the middle-IR apparent reflectance is investigated rigorously through the same radiative transfer model described above in section 2. Numerical computations were performed to demonstrate the linear relationship at the top of the atmosphere, given strict linear relations at the surface. For demonstration purposes we let the surface reflectance relationships for $0.49\text{--}2.2\ \mu\text{m}$ and $0.66\text{--}2.2\ \mu\text{m}$, given by *Kaufman et al.* [1997b],

$$\rho_{0.49\mu\text{m}} = 0.25\rho_{2.2\mu\text{m}}, \quad (11)$$

$$\rho_{0.66\mu\text{m}} = 0.5\rho_{2.2\mu\text{m}}. \quad (12)$$

Assuming (11) and (12), the resulting relationships at the top of the atmosphere are shown in Figure 4 for aerosol optical thickness values from zero to 1.2. For a given aerosol optical thickness, linear relations of reflectance are evident for both $0.49\text{--}2.2\ \mu\text{m}$ and $0.66\text{--}2.2\ \mu\text{m}$ at the top of the atmosphere. The apparent reflectance both at blue and red, for a given aerosol optical thickness, increases with the middle-IR reflectance. This shows the indirect impact of the surface on blue and red, since middle IR is relatively directly influenced by the surface. As aerosol optical thickness increases, the slope becomes flatter, showing less dependence on the surface reflectance.

For a given aerosol optical thickness, when the apparent middle-IR reflectance is small, the apparent reflectance of the blue band is much larger than that of the red band, even though the surface reflectance at red wavelengths is twice as big as that at blue wavelengths. This is primarily because of the large contribution of molecular scattering in the blue band. For small aerosol optical thickness, as the apparent middle-IR reflectance increases, the apparent reflectance at $0.66\ \mu\text{m}$ becomes larger than at $0.49\ \mu\text{m}$, making surface effects prominent. As aerosol optical thickness increases, surface contributions become less important. Hence for the same aerosol optical thickness the apparent reflectance of the blue band is larger than that of the red band, even if the latter has larger surface reflectance. The above comparison explains the radiative transfer model results. In reality, the aerosol optical thickness depends on wavelength in a complex way. The surface reflectances also vary spatially and temporally.

We conclude that for a horizontally uniform atmospheric aerosol, if the surface reflectances of the visible and the middle-IR bands are linearly correlated at the surface, the apparent reflectances at the top of the atmosphere are also linearly correlated. Furthermore, if we observe a linear correlation at the top of the atmosphere, we can also find a linear relation at the surface for a given aerosol optical thickness. Thus instead of pixel-by-pixel independent retrieval, we are led to consider a set of pixels that obey a linear correlation of visible and mid-IR apparent reflectance. These will also satisfy a linear visible and mid-IR relation at the surface and thus add another constraint to the retrieval process.

4. Observations and Retrieval Method

The theoretical analysis above demonstrates that the apparent reflectances in visible and middle IR are correlated if their counterparts are correlated at the surface. This information can be used to infer the aerosol optical thickness. On the basis of this physical principle we developed an atmosphere-surface coupled path radiance technique to retrieve aerosol optical

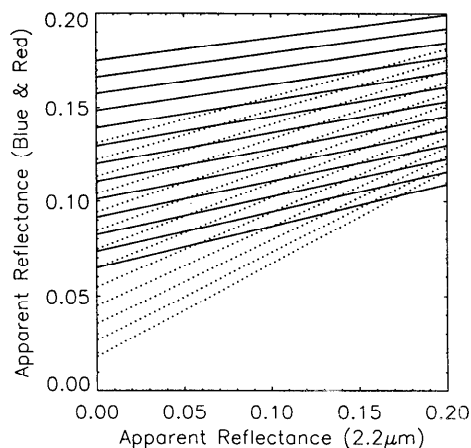


Figure 4. Relationships of apparent reflectance between middle IR at $2.2\ \mu\text{m}$ and visible bands at $0.49\ \mu\text{m}$ (solid), and $0.66\ \mu\text{m}$ (dotted) from radiative transfer calculation for different aerosol optical thickness from zero (bottom) to 1.2 (top) with an increment of 0.1. The relations in surface reflectance are assumed to be as in equations (11) and (12), with the atmosphere defined in Fig. 1.

thickness. In the following section we demonstrate the technique by applying it to a Landsat TM image.

4.1. Landsat Apparent Reflectance

Plate 1 presents scatterplots showing the $0.49\text{--}2.2\ \mu\text{m}$ and $0.66\text{--}2.2\ \mu\text{m}$ relations in a subsense of size of 512×512 pixels from a Landsat-5 TM image over the SGP site of the ARM program in Oklahoma, on September 27, 1997. For display purposes the scatterplots in Plate 1 sample every fourth pixel in the scene. The scene was acquired at about 1640 UTC with solar zenith angle of 44° . Both scatterplots appear to have linear correlation in the apparent reflectance, indicating the existence of a linear correlation at the surface as described in section 3. However, the range (maximum-minimum) is quite large, 0.03 for the blue band and 0.08 for the red band, for a given middle-IR reflectance.

Another feature is the increase of visible reflectance, particularly for the red band, as middle-IR reflectance approaches zero. This is due to spectral reflectance over standing water. Standing water almost completely absorbs radiation at middle-IR wavelengths, but reflects significantly in the visible.

The ground-based Sun photometer measurements are useful for validating satellite retrievals. The AERONET (Aerosol Robotic Network), which is an optical ground-based aerosol-monitoring network, has been developed and expanded in recent years [*Holben et al.*, 1998]. There were nearly 60 locations around the world contributing to the AERONET database in 1997. AERONET Sun photometer and other ground-based radiation measurements at the SGP site provide useful information to interpret the TM images.

On September 27, 1997, the sky over Oklahoma was very clear. The aerosol optical thickness observed by a Sun photometer of AERONET was less than 0.1 for wavelengths longer than $0.44\ \mu\text{m}$ throughout the day (Figure 5). In a rural area like SGP the horizontal variability of aerosol optical thickness is expected to be small. The time series of aerosol optical thickness observed by Sun photometer also indicates small spatial variability of aerosol optical thickness. The variability in visible reflectance for a given middle-IR reflectance in Plate 1

is likely related to the heterogeneous relationship of surface reflectance between the visible and the mid-IR spectrum. Detailed analysis of the variability of apparent reflectance and its relation to aerosol optical thickness variation is presented in section 4.3.

4.2. Locally Homogeneous Clusters

Theoretical analysis in section 3 shows that if surface reflectance in the visible is linearly correlated to mid-IR reflectance, then the apparent reflectance should also be linearly correlated. However, the surface reflectance is not always homogeneous. Different types of surfaces have different spectral characteristics. Even for surfaces of similar type, the subpixel variability can also affect spectral reflectance characteristics. To make use of the surface reflectance correlation signal and to filter out the noise, i.e., the pixels which do not have visible and mid-IR relations at the surface, the pixels need to come from relatively homogeneous surfaces.

The local homogeneity of a cluster of pixels may be measured by the mean $\bar{\alpha}$ and standard deviation σ of apparent reflectance of $N \times N$ pixels in the mid-IR band at $2.2 \mu\text{m}$. The standard deviation measures the local variability of reflectance. The selection criterion for homogeneous clusters is that the local standard deviation is small. We found that a threshold standard deviation of 0.02 is suitable to classify a cluster as homogeneous.

For a given threshold of standard deviation the number of homogeneous clusters decreases as the size of the cluster increases. Plate 2 presents the local means of reflectance of the visible bands and mid-IR band for homogeneous clusters of size ranging from 5×5 to 20×20 pixels from the subscene of Plate 1. With spatial homogeneous clusters in the middle IR, the blue band at $0.49 \mu\text{m}$ has smaller variability than the red band at $0.66 \mu\text{m}$ for a given mid-IR reflectance at $2.2 \mu\text{m}$. As the size of the local cluster increases, the variability of visible reflectances becomes smaller, as expected from the smaller number of homogeneous clusters in a given scene. However, the correlation is still evident for a cluster size of 20×20 pixels.

4.3. Variability of the Correlation

With the constraint of homogeneous clusters the linear correlation between the visible and the middle IR becomes more evident. The ranges of the visible reflectance of the original image, 0.03 for blue and 0.08 for red (Plate 1), are reduced to 0.01 and 0.03 for homogeneous clusters of size 10×10 pixels (Plate 2). Even though the linear relation of satellite-observed apparent reflectance can be explained as a combination of the atmospheric effect and the linear relation between visible and mid-IR surface reflectance, the variability in blue and red bands for a given reflectance at mid-IR band needs to be explored.

The AERONET Sun photometer observations show that aerosol optical thickness is very stable throughout the day. The change of aerosol optical thickness is less than 0.01 most of the time in any 15 min interval (Figure 5). The aerosol optical thickness of 0.01 may set an upper bound of spatial variability for any subscenes. The sensitivity study in section 2.2 (Figure 1), shows that the variability of apparent reflectance due to pure aerosol optical thickness variability is less than 0.001 in any subscene. Therefore the observed variability of apparent reflectance is primarily due to the variability in surface reflectance.

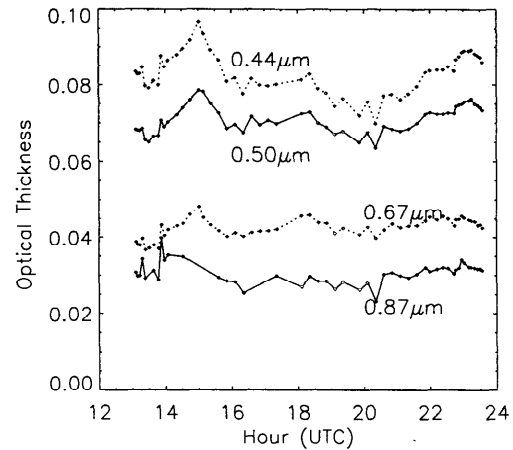


Figure 5. Aerosol optical thickness observed by Sun photometer at the SGP site of the ARM program on September 27, 1997, in visible bands at 0.44, 0.5, and 0.67 μm and a near-IR bands at 0.87 μm .

4.4. Aerosol Retrievals

Variability in surface reflectance affects apparent reflectance in two ways. First, even if restricted to locally homogeneous pixels, fluctuations of surface reflectance in the middle IR, hence the relationship between visible and middle IR, also appears at the top of the atmosphere. Second, the inhomogeneity of the surface reflectance in the whole scene introduces adjacency effects to locally homogeneous clusters through higher-order scattering processes [Tanré *et al.*, 1981; Mekler and Kaufman, 1980; Diner *et al.*, 1989]. Adjacency effects are expected to be smooth from pixel to pixel and become less important as the homogeneous cluster size increases. Here adjacency effects are not explicitly computed but may be estimated by varying cluster size, as in the previous section. For large enough clusters, the lower bound of linearly correlated scattered points describes the linear relation for the clusters that are darkest in the visible. Above this lower bound are the brighter surface clusters, which tend to mask the small aerosol signal. To extract the aerosol signal, the envelope of darkest homogeneous clusters is extrapolated to the intercept at which the middle IR vanishes. This is similar to the usual technique of extrapolating spectral transmissivity values with minimal aerosol contribution to the intercept at which precipitable water vanishes to determine molecular scattering transmissivity [e.g., Houghton, 1985, p. 79, Figure 3.7]. Here the envelope of dark surfaces is used to determine the intercept, which is then used to derive aerosol optical thickness.

In practice, to reduce the noise due to fluctuations of surface reflectance, the lower 20% of total homogeneous clusters is used to fit the envelope of the dark surfaces. A correlation coefficient of 0.8 of the linear fit is required to ensure the visible and mid-IR relation. Plate 3 presents example straight line fits to the lower bound envelope for a subscene of 512×512 pixels over the central facility site of SGP. The line is extrapolated to intercept the visible apparent reflectance with zero mid-IR reflectance. The linear relations in Plate 3 are typical for most of the subscenes.

For an atmosphere with strong correlation in apparent reflectance between the visible and the mid-IR spectra, the extrapolation of the best linear fit to zero mid-IR reflectance gives the path radiance of visible bands in reflectance units. In

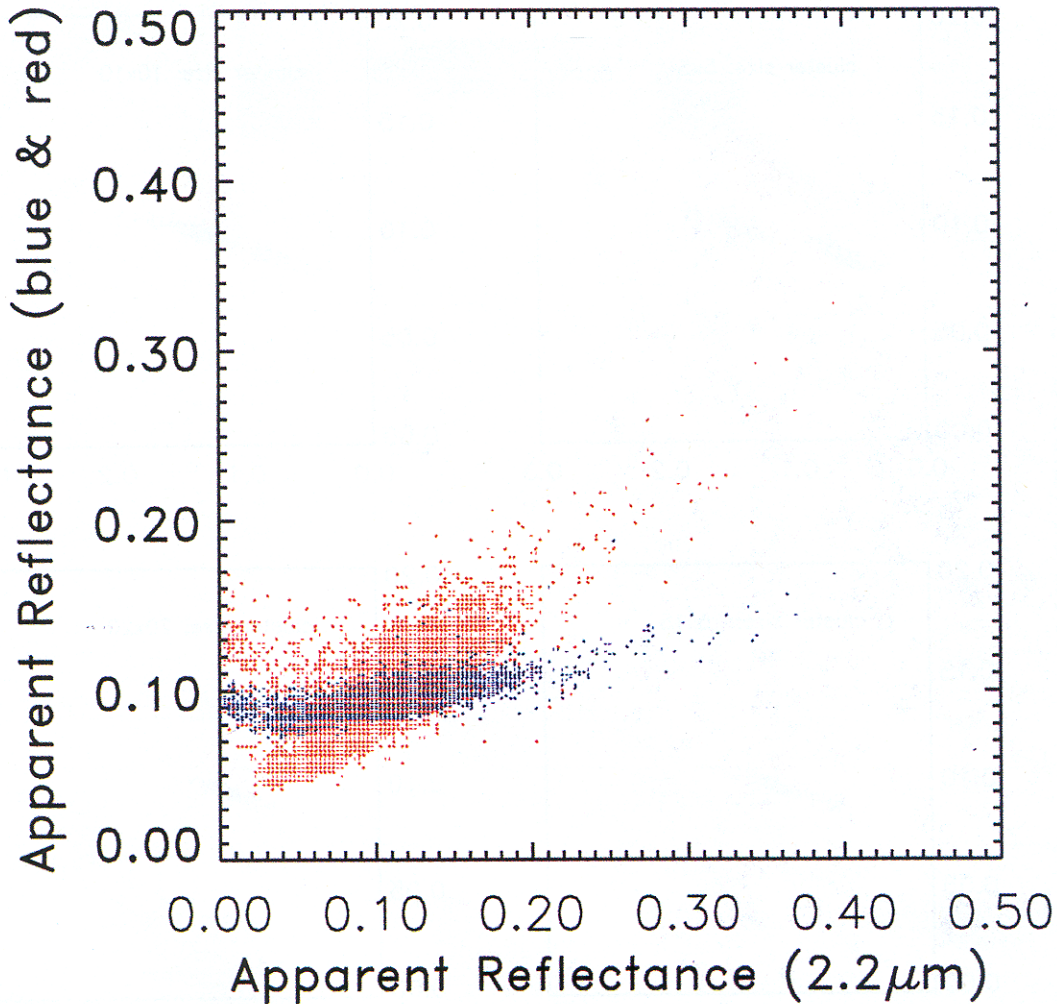


Plate 1. Scatterplots show the middle-IR and visible at $0.49 \mu\text{m}$ (blue), and middle-IR and visible at $0.66 \mu\text{m}$ (red) of apparent reflectance from a Landsat-5 TM subscene of 512×512 pixels on September 27, 1997, over the SGP site of the ARM program.

this way, we can decouple the atmospheric effect from the surface effect.

The amount of aerosol loading, together with Rayleigh scattering, determines the path radiance given by the intercept. From path radiance, atmospheric aerosol optical thickness can easily be retrieved.

5. Application and Error Analysis

To retrieve aerosol optical thickness from the whole Landsat TM scene, the image is divided into subscenes with size 512×512 pixels or about $15 \text{ km} \times 15 \text{ km}$ equivalently. In each of the subscenes the path radiance extrapolation technique described in section 4 is used to retrieve aerosol optical thickness. The statistics of aerosol optical thickness is examined and compared with that from “dark object” approach. Statistics of path radiance of the atmosphere are also given.

5.1. Comparison With the Dark Object Approach

A local homogeneous cluster size of 10×10 pixels is chosen to retrieve the aerosol optical thickness. A sensitivity study showing how the size of homogeneous clusters affects the aerosol optical thickness retrieval is presented below in section 5.3.

The frequency distribution of retrieved aerosol optical thickness from each subscene is plotted in Figure 6. The mean aerosol optical thickness is 0.09 and 0.07 with standard deviations 0.04 and 0.05 for the blue band and the red band, respectively. The distribution for the blue band is well behaved, while the distribution for the red band is positively skewed with larger dispersion. The larger uncertainty of the red band is related to a larger error propagation factor as explained in section 2.2 (see Fig. 3). The retrieved aerosol optical thickness agrees very well with the Sun photometer observed optical thickness, i.e., 0.07 and 0.04 for blue and red band, respectively (Figure 5).

The histogram of the aerosol optical thickness of the same image retrieved from the “dark object” approach [Liang *et al.*, 1997] is presented in Figure 7. “Dark objects” are defined as pixels with apparent reflectance in mid-IR less than 0.1 and NDVI greater than 0.1, where NDVI is defined as

$$\text{NDVI} = \frac{\alpha_{0.8\mu\text{m}} - \alpha_{0.66\mu\text{m}}}{\alpha_{0.8\mu\text{m}} + \alpha_{0.66\mu\text{m}}}, \quad (13)$$

where $\alpha_{0.66 \mu\text{m}}$ and $\alpha_{0.8 \mu\text{m}}$ are apparent reflectances of TM bands 3 and 4, respectively. The surface reflectance relationships in (11) and (12) are used.

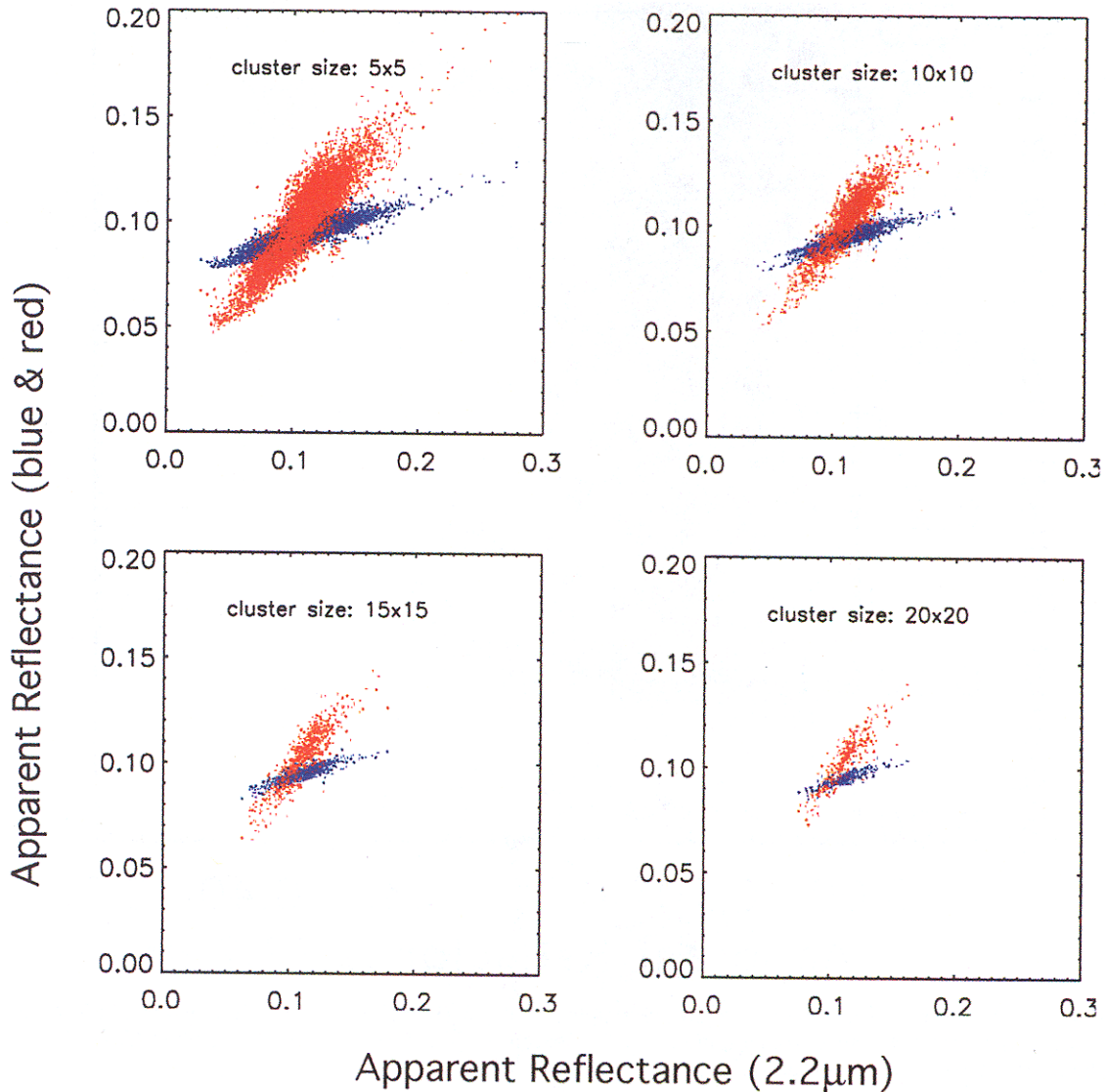


Plate 2. From the same subsene in Plate 1 the scatterplots show the middle IR and visible at $0.49 \mu\text{m}$ (blue), and mid-IR and visible at $0.66 \mu\text{m}$ (red) relations of apparent reflectance for homogeneous clusters of different sizes ranging from 5×5 to 20×20 pixels.

The dark object approach gives aerosol optical thickness of 0.08 and 0.30 with standard deviation of 0.07 and 0.16 for blue and red band, respectively. The aerosol optical thickness of the blue band from the dark object approach agrees with the Sun photometer measurements quite well. However, the dark object approach greatly overestimates aerosol optical thickness by 0.26 in absolute value (or a factor of 7) for the red band. This clearly indicates that the red and mid-IR relationships are not adequate for this scene. The large standard deviation of aerosol optical thickness in the red band is associated with large variability of red band surface reflectance for a given mid-IR reflectance, as described in section 2.2.

5.2. Path Radiance

Retrieved aerosol optical thickness depends on the aerosol model. The uncertainties related to the aerosol model are very difficult to examine in an absolute sense because of the dearth of observations of microphysical properties, chemical composition, and even geometrical shape of aerosol particles [Wis-

combe and Mugnai, 1988; Mishchenko *et al.*, 1997]. Good agreement between satellite-retrieved aerosol optical thickness and Sun photometer measurements does not necessarily validate the technique. Another way to examine the technique without involving the aerosol model is to investigate the distribution of path radiance as measured by the intercept of the straight line fit.

The path radiance is the backscattered radiation from the atmosphere that has not interacted with the surface. For a horizontally stratified atmosphere the path radiance is expected to be nearly constant within the Landsat TM scene. The dispersion of the distribution determines the reliability of the technique. Figure 8 presents the distribution of the path radiances for both blue and red bands with a homogeneous cluster size of 10×10 . The mean path radiances are 0.073 and 0.024 with standard deviations of 0.004 and 0.005 for the blue and red band, respectively. The variability of the path radiances measured by the standard deviation are only three digital radiance counts of Landsat-5 TM for both blue and red bands,

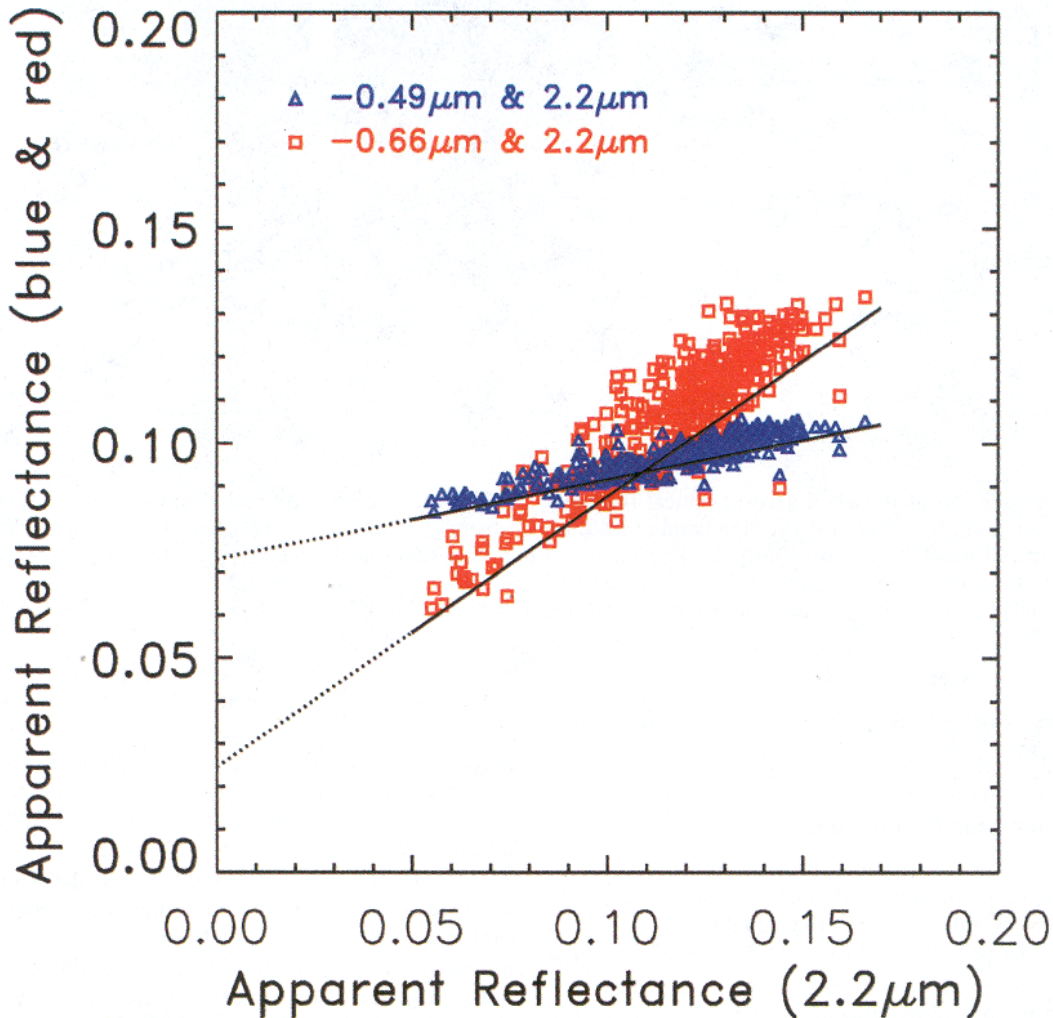


Plate 3. Scatterplots show the mid-IR and visible at $0.49 \mu\text{m}$ (blue), and mid-IR visible at $0.66 \mu\text{m}$ (red) relations for a homogeneous cluster size of 10×10 pixels from a subsene of 512×512 pixels. The straight line fits the lower 20% of the scattered points.

indicating that the mean values of the intercepts truly represent the path radiances of the atmosphere.

5.3. Size of Homogeneous Clusters

The size of homogeneous clusters can affect aerosol optical thickness retrieval in two ways. As the size of the homogeneous cluster increases, the adjacency effect becomes less important. However, the number of such clusters would decrease if the homogeneity level, i.e., the local standard deviation, is kept the same. The smaller number of homogeneous clusters statistically increases the uncertainty level of the mean aerosol optical thickness. It is interesting to investigate how the size of local homogeneous clusters affects the aerosol optical thickness retrieval.

As above, the whole scene is divided into subsenes with a size of 512×512 pixels. The retrieved aerosol optical properties from each subsene is used to calculate the mean and standard deviation with a varying size of local homogeneous clusters ranging from 3×3 to 20×20 pixels (or from $90 \text{ m} \times 90 \text{ m}$ to $600 \text{ m} \times 600 \text{ m}$).

The mean and standard deviation of aerosol optical thickness from the TM scene are presented in Figure 9. It is clear

that changes in the mean of optical thickness for both blue and red bands with cluster size are small compared to the standard deviation. A small smooth decrease of the mean aerosol optical thickness of the blue band with the increase of cluster size is evident. The decrease of the retrieved aerosol optical thickness of the blue band with the size of the local homogeneous cluster is likely related to the decrease of adjacency effect. Nevertheless, the effect of the size of local homogeneous clusters is within the statistical uncertainty as measured by the standard deviation.

The standard deviation increases from 0.04 to 0.05 for the blue band, and from 0.05 to 0.09 for the red band as the size increases from 90 to 600 m. The increase in the variability is likely related to the statistical decrease in the number of homogeneous clusters. The larger uncertainty of the red band as the homogeneous cluster size increases indicates the greater sensitivity of the red band apparent reflectance on the surface reflectance. The path radiance of the blue band has a smooth decrease as the size of the local homogeneous cluster increases, similar to the retrieved aerosol optical thickness. The standard deviation of the path radiance is about 0.005 for blue. However, the standard deviation of path radiance for red band

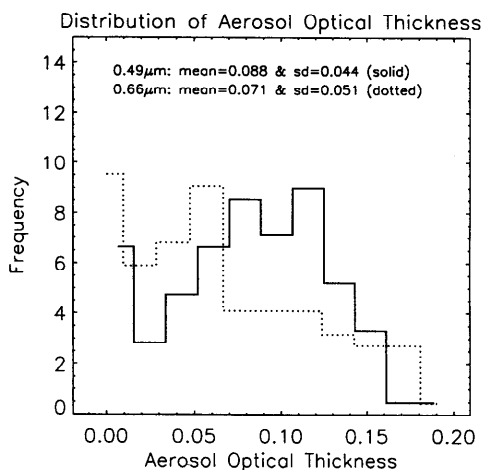


Figure 6. Distribution of retrieved aerosol optical thickness by the “path radiance” technique for the blue band at $0.49 \mu\text{m}$ (solid) and the red band at $0.66 \mu\text{m}$ (dotted). The means of aerosol optical thickness are 0.088 and 0.071, with a standard deviation of 0.044 and 0.051, for the blue and red bands, respectively.

increases from 0.005 to 0.009 as the size increases from 90 to 600 m.

6. Summary and Discussion

The retrieval of aerosol properties using satellite-observed reflected solar radiation must minimize the noise from background surfaces in order to detect the signal from aerosols. A sensitivity study was performed here in order to estimate the relative contribution of aerosols and surfaces and to understand how errors in surface reflectance affect the aerosol optical thickness retrieval. The apparent reflectance is very sensitive to the change of surface reflectance when aerosol optical thickness is small. The change in apparent reflectance is greater than a factor of 0.65 of the change in surface reflectance, given an aerosol optical thickness less than 0.5 for both blue and red bands. Uncertainties in surface reflectance estimation lead to significant errors in aerosol optical thickness retrievals especially when aerosol optical thickness is small. The error in aerosol optical thickness is about 5–20 times the error in surface reflectance for aerosol optical thickness less than 2 and surface reflectance less than 0.12. The large error propagation factor (10–20 for optically thin aerosol, thickness less than 0.1 for example) introduces large errors in aerosol optical thickness retrievals.

A “path radiance” algorithm to retrieve aerosol optical thickness over land is presented. The path radiance technique is based on the fact that the visible (blue and red) and mid-IR reflectance are linearly correlated for wet soil and vegetated surfaces. The signature of visible and mid-IR linear correlation at the surface implies a similar correlation in apparent reflectance at the top of the atmosphere if the atmosphere is horizontally stratified. This information is used to retrieve aerosol optical thickness.

The path radiance technique is applied to a TM image over the Oklahoma SGP site of the ARM program, taken on September 27, 1997, during the first Landsat IOP of the ARM program. The retrieved aerosol optical thickness (0.09 and 0.07 for the blue and red bands, respectively, with uncertainty of

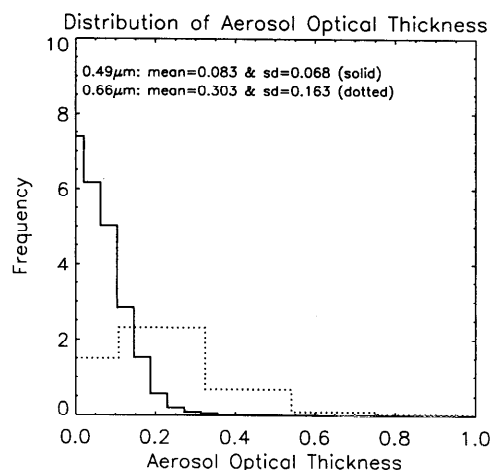


Figure 7. Aerosol optical thickness retrieved by the “dark object” technique, for the same scene as in Fig. 6. The means of aerosol optical thickness are 0.083 and 0.303, with standard deviation of 0.068 and 0.163, for the blue (solid) and red (dotted) bands, respectively.

0.05) is in good agreement with Sun photometer measurements (optical thickness of 0.07 and 0.04 for blue and red bands, respectively). The relatively large uncertainty (0.05 compared to typical Sun photometer uncertainty less than 0.01) reflects the noise from the surface. The “dark object” approach is also applied to the same scene. The optical thickness of the blue band retrieved by the dark object method agrees quite well with the ground-based Sun photometer measurements. However, the dark object technique largely overestimates the aerosol optical thickness in the red band by 0.26 in absolute value (or a factor of 7), indicating that the standard correlation between red and mid-IR, determined from data in other geographic regions, is not appropriate for this scene.

In the method recommended here, path radiance is retrieved as the intercept of an extrapolated linear fit of visible and mid-IR top-of-the-atmosphere reflectances. The variability

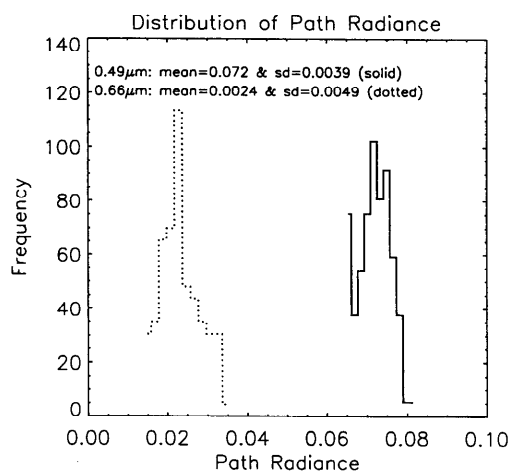


Figure 8. Distribution of path radiance measured by the intercepts of linear line fits. The averaged path radiance is 0.0725 and 0.0241, with standard deviations of 0.0039 and 0.0049, for the blue at $0.49 \mu\text{m}$ (solid) and red at $0.66 \mu\text{m}$ (dotted) bands, respectively. The homogeneous cluster size is 10×10 pixels.

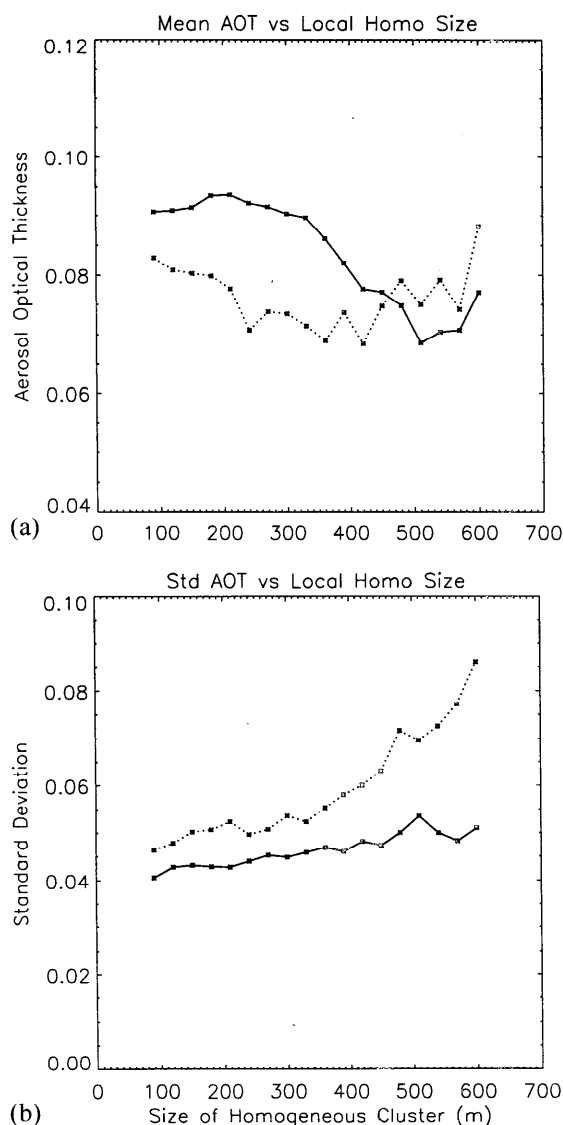


Figure 9. Retrieved (top) mean aerosol optical thickness and (bottom) standard deviation for different homogeneous cluster sizes ranging from 3×3 to 20×20 pixels for the blue band (solid), or from $90\text{m} \times 90\text{m}$ to $600\text{m} \times 600\text{m}$ for the red band (dotted), respectively.

ity of the path radiance is small and independent of the aerosol microphysical properties and chemical composition. In the example given here, the standard deviations of 0.004 and 0.006 for the path radiance of blue and red bands are very small, about three digital radiance counts of Landsat-5 TM imagery. The larger variability for the red band is likely related to a larger variability of red and mid-IR relation and the larger sensitivity of apparent reflectance to surface reflectance in this band.

The retrieved aerosol optical thickness is quite stable as the size of local homogeneous clusters increases. Again, the larger uncertainty in the red band is associated with the larger error propagation factor. A smooth decrease of the blue band aerosol optical thickness with the increase of homogeneous cluster size is likely due to adjacency effects. The uncertainty associated with the size of local homogeneous clusters is within the

statistical uncertainty measured by the standard deviation for both blue and red bands.

The physics of the path radiance retrieval scheme is simple and easy to apply. The path radiance procedure is summarized as follows: (1) construct the linear relation of apparent reflectance between a particular visible band and the mid-IR band using local homogeneous clusters; (2) fit a straight line to the bottom of the envelope of the scatter relation; (3) determine the intercept of the straight line, i.e., the value of the visible radiance for which the mid-IR radiance vanishes. This intercept describes the chosen visible band atmospheric path radiance, from which the corresponding aerosol optical thickness is retrieved. Since the technique is one-dimensional plane parallel retrieval, it may not work properly when the aerosol layer is not uniform (e.g., smoke plume), or where the surface reflectance has large contrast (e.g., near the coastline).

The path radiance technique implicitly uses the visible and mid-IR surface reflectance correlations (where they are valid). It avoids using specific values of these relations as the traditional dark object approach does. Therefore the aerosol optical thickness retrievals and the surface visible and mid-IR reflectance relations are self-consistently embedded. Since the aerosol layer is optically thin in many geographic locations at most times, the ability to retrieve small aerosol optical thickness makes this technique promising. The technique has been applied to only one Landsat TM scene so far. Further research is under way to validate the technique and to investigate the extent of land surfaces where the visible and mid-IR reflectances are correlated.

Acknowledgments. The authors are especially grateful to the Department of Energy ARM personnel for helping to make the Landsat IOP field project and data collection a success. This research was supported by funding provided under NASA Landsat Science Team activities, which is part of NASA-MTPE, under proposal 1996-MTPE-00116, and the Department of Energy ARM program, under grant DE-AI02-97ER62369. One of the authors (SCT) would like to thank the support from the NASA Radiation Science Program, managed by Robert J. Curran, for developing models used in this study.

References

- d'Almeida, G. A., P. Koepke, and E. P. Shettle, Atmospheric aerosols, in *Global Climatology and Radiative Characters*, 420 pp., A Deepak, Hampton, Va., 1991.
- Diner, D. J., and J. V. Martonchik, Influence of aerosol scattering on atmospheric blurring of surface features, *IEEE Trans. Geosci. Remote Sens.*, 23, 618–624, 1985.
- Diner, D. J., J. V. Martonchik, E. D. Danielson, and C. J. Brugge, Atmospheric corrections of high resolution land surface images, in paper presented at the IGARSS'89 Symposium and the Twelfth Canadian Symposium on Remote Sensing, Int. Geosci. and Remote Sens. Symp., Vancouver, B. C., Canada, 1989.
- Evans, K. F., The spherical harmonics discrete ordinate method for three-dimensional atmospheric radiative transfer, *J. Atmos. Sci.*, 55, 429–446, 1998.
- Ferrare, R. A., R. S. Fraser, and Y. J. Kaufman, Satellite remote sensing of large-scale air pollution: Measurements of forest fire smoke, *J. Geophys. Res.*, 95, 9911–9925, 1990.
- Fraser, R. S., Satellite measurement of mass of Sahara dust in the atmosphere, *Appl. Opt.*, 15, 2471–2479, 1976.
- Fraser, R. S., Y. J. Kaufman, and R. L. Mahoney, Satellite measurements of aerosol mass and transport, *Atmos. Environ.*, 18, 2577–2584, 1984.
- Fraser, R. S., R. A. Ferrare, Y. J. Kaufman, B. L. Markham, and S. Mattoo, Algorithm for atmospheric correction of aircraft and satellite imagery, *Int. J. Remote Sens.*, 13, 541–557, 1992.
- Gordon, H., and M. Wang, Retrieval of water-leaving radiance and

- aerosol optical thickness over the oceans with SeaWiFS: A preliminary algorithm, *Appl. Opt.*, 33, 443–452, 1994.
- Griggs, M., Satellite measurements of tropospheric aerosols, *Adv. Space Res.*, 2, 109–118, 1983.
- Holben, B. N., et al., AERONET—A federated instrument network and data archive for aerosol characterization, *Remote Sens. Environ.*, 66, 1–16, 1998.
- Houghton, H. G., *Physical Meteorology*, 442 pp., MIT Press, Cambridge, Mass., 1985.
- Intergovernmental Panel on Climate Change (IPCC), *Aerosol Radiative Forcing and Climate Change*, 161 pp., Natl. Acad. Press, Washington, D. C., 1996.
- Kaufman, Y. J., and C. Sendra, Algorithm for automatic atmospheric corrections to visible and near-IR satellite imagery, *Int. J. Remote Sens.*, 9, 1357–1381, 1988.
- Kaufman, Y. J., R. Fraser, and R. Ferrare, Satellite measurements of large-scale air pollution: Method, *J. Geophys. Res.*, 95, 9895–9909, 1990.
- Kaufman, Y. J., D. Tanré, H. R. Gordon, T. Nakajima, J. Lenoble, R. Frouin, H. Grassl, B. M. Herman, M. D. King, and P. M. Teillet, Passive remote sensing of tropospheric aerosol and atmospheric correction for the aerosol effect, *J. Geophys. Res.*, 102, 16,815–16,830, 1997a.
- Kaufman, Y. J., A. E. Wald, L. A. Remer, B.-C. Gao, R.-R. Li, and L. Flynn, The MODIS 2.1- μm channel correlation with visible reflectance for use in remote sensing of aerosol, *IEEE Trans. Geosci. Remote Sens.*, 35, 1286–1298, 1997b.
- Kaufman, Y. J., D. D. Herring, K. J. Ranson, and G. J. Collatz, Earth observing system AM1 mission to Earth, *IEEE Trans. Geosci. Remote Sens.*, 36, 1045–1055, 1998.
- Kästner, M., P. Köpke, and H. Quenzel, Monitoring of Saharan dust over the Atlantic using Meteosat-Vis-Data, *Adv. Space Res.*, 2, 119–121, 1983.
- Köpke, P., and H. Quenzel, Turbidity of the atmosphere determined from satellite: Calculation of optimum viewing geometry, *J. Geophys. Res.*, 84, 7847–7856, 1979.
- Köpke, P., and H. Quenzel, Turbidity of the atmosphere determined from satellite: Calculation of optimum wavelength, *J. Geophys. Res.*, 86, 9801–9805, 1981.
- Liang, S., H. Fallah-Adl, S. Kalluri, J. J. J. Kaufman, and J. R. G. Townshend, An operational atmospheric correction algorithm for Landsat Thematic Mapper imagery over the land, *J. Geophys. Res.*, 102, 17,173–17,186, 1997.
- Liou, K.-N., *An Introduction to Atmospheric Radiation*, Academic, San Diego, Calif., 1980.
- Markham, B. L., and J. L. Barker, Spectral characterization of the Landsat Thematic Mapper sensors, *Int. J. Remote Sens.*, 6, 697–716, 1985.
- Mekler, Y., and Y. J. Kaufman, The effect of Earth's atmosphere on contrast reduction for nonuniform surface albedo and two-halves field, *J. Geophys. Res.*, 85, 4067–4083, 1980.
- Mekler, Y., H. Quenzel, G. Ohring, and I. Marcus, Relative atmospheric aerosol content from Erts observations, *J. Geophys. Res.*, 82, 967–970, 1977.
- Mishchenko, M., L. D. Travis, R. A. Kahn, and R. A. West, Modeling phase functions for dustlike tropospheric aerosols using a shape mixture of randomly oriented polydisperse spheroids, *J. Geophys. Res.*, 102, 16,831–16,847, 1997.
- Nakajima, T., and A. Higurashi, AVHRR remote sensing of aerosol optical properties in the Persian Gulf region, summer 1991, *J. Geophys. Res.*, 102, 16,935–16,946, 1997.
- Otterman, J., and R. S. Fraser, Adjacency effects on imaging by surface reflection and atmospheric scattering: Cross radiance to zenith, *Appl. Opt.*, 18, 2852–2860, 1979.
- Shettle, E. P., and R. W. Fenn, Models for the aerosols of the lower atmosphere and the effects of humidity variations on their optical properties, *AFGL-TR-79-0214*, *Environ. Res. Pap.* 675, 94 pp., Natl. Tech. Inf. Serv., Springfield, Va., 1979.
- Stamnes, K., S.-C. Tsay, W. Wiscombe, and K. Jayaweera, Numerically stable algorithm for discrete-ordinate-method radiative transfer in multiple scattering and emitting layered media, *Appl. Opt.*, 27, 2502–2509, 1988.
- Stowe, L. L., A. M. Ignatov, and R. R. Singh, Development, validation, and potential enhancements to the second-generation operational aerosol product at the National Environmental Satellite, Data and Information Service of the National Oceanic and Atmospheric Administration, *J. Geophys. Res.*, 102, 16,923–16,934, 1997.
- Tanré, D., M. Herman, and P. Y. Deschamps, Influence of the background contribution upon space measurements of ground reflectance, *Appl. Opt.*, 20, 3673–3684, 1981.
- Tanré, D., Y. J. Kaufman, M. Herman, and S. Mattoo, Remote sensing of aerosol properties over oceans using the MODIS/EOS spectral radiances, *J. Geophys. Res.*, 102, 16,971–16,988, 1997.
- Tsay, S.-C., K. Stamnes, and K. Jayaweera, Radiative transfer in stratified atmospheres: Development and verification of a unified model, *J. Quant. Spectrosc. Radiat. Transfer.*, 43, 133–148, 1990.
- Tsay, S.-C., G. L. Stephens, and T. Greenwald, An investigation of aerosol microstructure on visual and air quality, *Atmos. Environ.*, 25(A), 1039–1053, 1991.
- Wiscombe, W. J., and A. Mugnai, Scattering from nonspherical Chebyshev particles. 2. Means of angular scattering patterns, *Appl. Opt.*, 27, 2405–2421, 1988.

R. F. Cahalan, L. Oreopoulos, S.-C. Tsay, and G. Wen, NASA Goddard, Climate and Radiation Branch, Code 913, Greenbelt, MD 20771. (wen@climate.gsfc.nasa.gov)

(Received March 2, 1999; revised July 19, 1999; accepted August 31, 1999.)